ELSEVIER

Journal of Organometallic Chemistry 565 (1998) 81–95

Journal of Organometallic Chemistry

Mixed-metal cluster chemistry IX[1]: alkylarylphosphine derivatives of $[CpWIr_3(CO)_{11}]$ and X-ray crystal structure of $[CpWIr_3(\mu\text{-}CO)_3(CO)_7(PMe_2Ph)]$[2]

Susan M. Waterman [a], Mark G. Humphrey [a,*], David C.R. Hockless [b]

[a] *Department of Chemistry, Australian National University, Canberra, ACT 0200, Australia*
[b] *Research School of Chemistry, Australian National University, Canberra, ACT 0200, Australia*

Received 25 November 1997

Abstract

Reactions of $[CpWIr_3(CO)_{11}]$ (**1**) with equimolar amounts of the bidentate alkylarylphosphines bis(diphenylphosphino)ethane (dppe) and bis(diphenylphosphino)methane (dppm) afford the substitution products $[CpWIr_3(\mu\text{-}L)(\mu\text{-}CO)_3(CO)_6]$ [L = dppe (**2**), dppm (**3**)]. Reactions of **1** with stoichiometric amounts of the monodentate alkylarylphosphines $PMePh_2$ and PMe_2Ph afford the substitution products $[CpWIr_3(\mu\text{-}CO)_3(CO)_{8-n}(L)_n]$ [L = $PMePh_2$, $n = 1$ (**4**), 2 (**5**), 3 (**6**); L = PMe_2Ph, $n = 1$ (**7**), 2 (**8**), 3 (**9**)]. The clusters **2–8** are fluxional in solution, with the interconverting isomers resolvable at low temperatures. Variable temperature ^{31}P- and ^{13}C-NMR spectra for **2** and **3** enable structural assignment of the isomers, revealing a triiridium face spanned by bridging carbonyls, a diaxially-ligated diphosphine with (in the case of dppe) a flexible backbone, and an apical tungsten-coordinated cyclopentadienyl (Cp) ligand situated over differing WIr_2 faces in the configurations. ^{13}C-NMR exchange spectroscopy (EXSY) spectra reveal that these isomers interconvert by tripodal rotation at the apical $CpW(CO)_2$, resolvable (in the case of **3**) into a 'waggling' of the $CpW(CO)_2$ group over the non-diphosphine ligated WIr_2 faces before the onset of complete tripodal rotation. A 'merry-go-round' of carbonyl ligands in the basal $Ir(\mu\text{-}CO)_3(CO)_3$ plane occurs at a similar temperature to that of tripodal rotation for **3**, but at a higher temperature for **2**. For **2**, flexing of the diphosphine backbone is the highest energy process observed. A structural study of one isomer of **7**, namely **7a**, reveals that the three edges of the triiridium face of the tetrahedral core are spanned by bridging carbonyls, and that the iridium-bound PMe_2Ph ligates axially and the tungsten-bound Cp coordinates apically with respect to the triiridium face. Information from this crystal structure, ^{31}P-NMR data, and comparison with analogous PPh_3- and PMe_3-ligated tungsten–triiridium clusters have been employed to suggest coordination geometries for the other isomers of **4–9**. The geometries of the $PMePh_2$- and PMe_2Ph-derivatives **4-9** follow those of the previously reported PMe_3-derivatives, with the exception of the minor isomer $[CpWIr_3(\mu\text{-}CO)_3(CO)_5(PMePh_2)_3]$ (**6b**) which has an unprecedented triradial, apical substitution geometry.

Keywords: Tungsten; Iridium; Carbonyl; Cyclopentadienyl; Cluster; Fluxionality; Phosphine; Crystal structure

1. Introduction

There has been considerable interest in the chemistry of mixed-metal clusters [2], with many reports focusing on ligand substitution [1]. Our investigations in this area have involved molybdenum–iridium and tungsten–iridium clusters [1,3–9]. As part of these studies we recently reported the substitution of $[CpWIr_3(CO)_{11}]$ (**1**) by stoichiometric amounts of PPh_3 or PMe_3 [4].

* Corresponding author. Tel.: +61 2 62492927; fax: +61 2 62490760; e-mail: Mark.Humphrey@anu.edu.au

[1] See ref. [1].

[2] Dedicated to Professor Michael Bruce on the occasion of his 60th birthday, in recognition of his many important contributions to organometallic chemistry. M.G. Humphrey thanks Michael for encouraging his development as an organometallic apprentice and for his continuing support.

0022-328X/98/$19.00
PII S0022-328X(98)00445-8

Some of the products of the reactions, namely [CpWIr$_3$(μ-CO)$_3$(CO)$_{8-n}$(L)$_n$] (L = PPh$_3$, n = 1 or 2; PMe$_3$, n = 1 or 2), exhibit ligand fluxionality in solution, resolvable at low temperatures into the constituent interconverting isomers; the isomers postulated for the mono- and tris-PPh$_3$ substituted clusters are different to those of their PMe$_3$ substituted analogues. We have therefore been prompted to investigate the steric and electronic factors directing the isomer distribution, and have consequently extended our studies to embrace phosphines with steric demands and electronic effects between those of PPh$_3$ or PMe$_3$. We report herein the reactivity of **1** toward one, two or three equivalents of PMePh$_2$ or PMe$_2$Ph, the characterisation by a single-crystal X-ray study of one isomer of the mono-PMe$_2$Ph derivative, and the identification of the other isomeric derivatives.

It is also of interest to compare the chemistry of the monodentate alkyldiarylphosphine PMePh$_2$ with that of its bidentate analogues bis(diphenylphosphino)methane (dppm) and bis(diphenylphosphino)ethane (dppe). Some time ago we reported the syntheses and X-ray structural characterisations of [CpWIr$_3$(μ-L)(μ-CO)$_3$(CO)$_6$] (L = dppe, dppm) [3]. In light of our discovery of interconverting isomers for the monodentate phosphine adducts, we have reinvestigated the bidentate phosphine complexes, and report herein their variable temperature ^{13}C- and ^{31}P-NMR spectra which reveal the presence of interconverting isomers, one of which (in each case) has the crystallographically-identified geometry. We also report ^{13}C-NMR exchange spectroscopy (EXSY) studies which have enabled us to elucidate the pathways for ligand fluxionality in these complexes.

2. Results and discussion

2.1. NMR spectra of complexes 2 and 3

We have previously described the syntheses of [CpWIr$_3$(μ-dppe)(μ-CO)$_3$(CO)$_6$] (**2**) and [CpWIr$_3$(μ-dppm)(μ-CO)$_3$(CO)$_6$] (**3**) [3]. We have now carried out variable temperature ^{31}P- and ^{13}C-NMR spectroscopic studies of **2**, the results of which are displayed in Figs. 1 and 2.

The ^{31}P-NMR spectrum of **2** in CDCl$_3$ at 323 K consists of a broad singlet at −14.7 ppm (Fig. 1). On cooling to 193 K (in CD$_2$Cl$_2$), six signals are resolved, corresponding to the presence of three isomers in the ratio 1.00:0.40:0.01. Similarly, the ^{13}C-NMR spectrum of **2** at 323 K shows a single peak at 173 ppm, but at 193 K the fluxional processes are sufficiently slow to distinguish resonances corresponding to three different isomers (Fig. 2); the least abundant isomer becomes visible upon applying a line broadening of 10 Hz to the ^{13}C-NMR spectrum at 193 K, to enhance the signal:noise ratio. The chemical shifts of the two most abundant isomers in the ^{31}P-NMR spectrum suggest that they are very similar to each other. One configuration of complex **2** has been structurally characterised; with respect to the carbonyl-bridged triiridium plane, it has a diaxially-ligated diphosphine and an apically coordinated cyclopentadienyl (Cp) ligand [3]. The NMR spectra suggest the presence of the three isomers displayed in Fig. 3a, one of which has the structurally characterised configuration. Isomers **2a** and **2b** are similar, having the Cp ligand inclined to the WIr$_2$ faces remote from the diphosphine, whereas the postulated structure for minor isomer **2c** has the Cp inclined to the WIr$_2$ face adjacent to the diphosphine. Isomers **2a** and **2b** differ in the conformation of the diphosphine backbone with respect to the location of the Cp ligands. Isomer **2b** is the crystallographically-observed form, with the methylene attached to the phosphorus which is ligated to an iridium in the WIr$_2$ face containing the Cp ligand being 'out' rather than 'in' (see Fig. 3b).

Extending the NMR chemical shift positional sequence established with tetrairidium clusters (bridging > radial > axial ≈ apical [10]) to the mixed-metal regime affords the chemical shift sequence W–W bridging CO > W–Ir bridging CO > Ir–Ir bridging CO ≈ W terminal CO > Ir radial CO > Ir axial CO ≈ Ir apical CO; it is possible to distinguish Ir–Ir bridging CO's from W terminal CO's due to the 15% abundant ^{183}W-coupled satellites of the latter. With this information, it is then possible to assign the spectrum of **2a**–**c**. At 193 K, resonances for the most abundant isomer (**2a**) are observed at 221.5 (e), 215.0 (c or d), 212.4 (a or b), 211.0 (b or a), 207.0 (d or c), 181.0 (f or g), 180.5 (g or f), 176.0 (h) and 161.0 (i) ppm, all of relative intensity 1, with the signals at 212.4 and 211.0 ppm showing the expected satellite coupling to ^{183}W. An attempt to establish the assignments of a and b from the possible presence of long-range *trans* coupling from a to i in a complementary ^{13}C–^{13}C correlation spectroscopy (COSY) experiment was unsuccessful. Fortunately, however, a more precise assignment of a or b is of no importance for the discussion of the fluxionality of **2**. The signals at 181.0, 180.5 and 176.0 ppm are assigned to the radial carbonyls f or g, g or f, and h, respectively, due to the similar chemical environments of the first two. Again, a precise assignment of f and g is not required to understand the fluxional processes of **2**. The signal at 221.5 ppm is assigned to bridging carbonyl e, by analogy to the assignment of the equivalent carbonyl in isomer **3b**: see below. Carbonyls c and d cannot be distinguished based on available information. Resonances for the least abundant isomer (**2c**) are observed at 227.9 (*c*), 210.1 (*a*, *a*′), 204.5 and 203.3 (*b*, *b*′), 179.5 and 178.9 (*d*, *d*′), 178.1 (*e*) and 167.7 (*f*) ppm, with

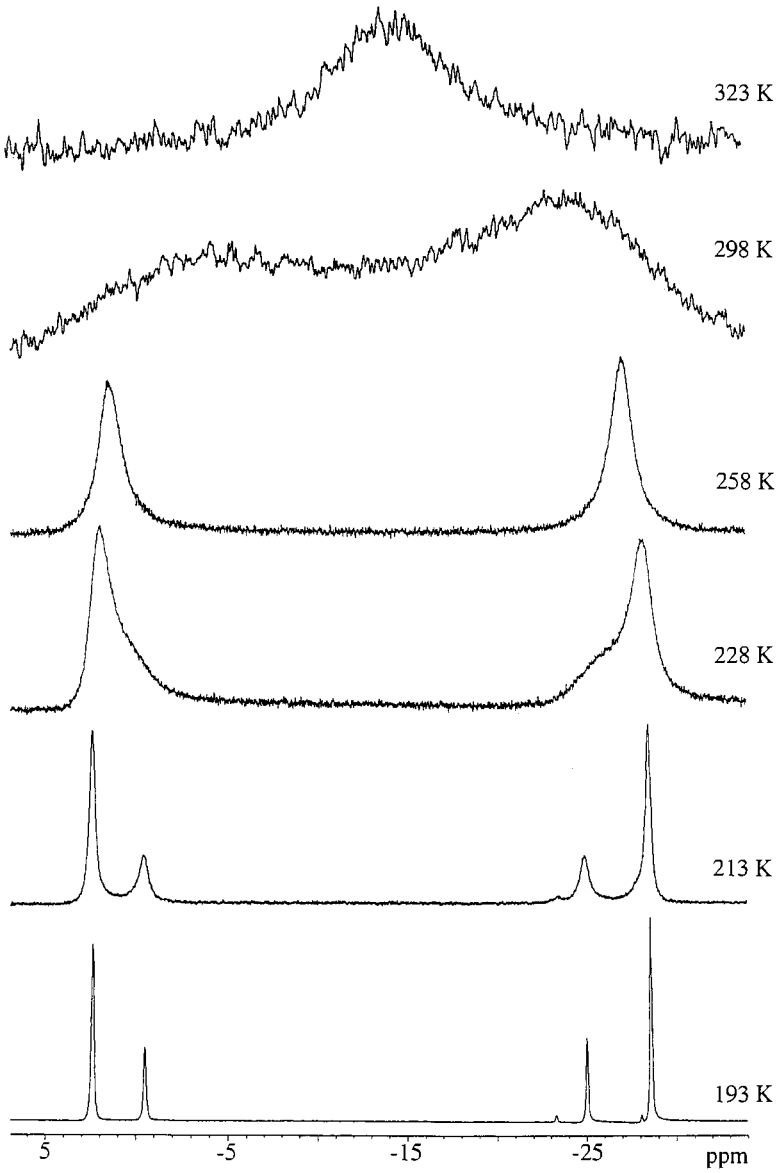

Fig. 1. Variable temperature ^{31}P-NMR spectroscopic study of [CpWIr$_3$(μ-dppe)(μ-CO)$_3$(CO)$_6$] (**2**).

relative intensities 1:2:1:1:1:1:1:1. The dppe backbone methylenes, one of which is 'out', the other of which is 'in' (Fig. 3b), result in slightly different magnetic environments for *d* and *d′* and for *b* and *b′*, an effect which is attenuated for the more remote *a* and *a′* resulting in the sole signal of intensity 2. The specific assignments follow those outlined above for the most abundant isomer. Signals for isomer **2b** are observed at 220.5 (E), 211.2 (A), 210.7 (C or D), 209.0 (D or C), 181.8 (F or G), 180.2 (G or F), 176.0 (H), and 162.2 (I) ppm, all of relative intensity 1, assigned analogously to isomer **2a**. In the figures, an arbitrary assignment has been adopted for carbonyl resonances which cannot be unambiguously assigned, to enhance clarity of presentation; it does not affect arguments regarding ligand fluxionality.

Ligand fluxionality commences upon warming the mixture of isomers of **2**. A ^{13}C{^{1}H}-EXSY study at 208 K is shown in Fig. 4. EXSY experiments use a NOESY sequence which allows for a 'mixing time' during which the observed nuclei may migrate to another site. The off-diagonal cross-peaks in the 2-D experiment occur between the shifts of exchanging sites [11]. The contour plot for cluster **2** shown in Fig. 4 reveals site exchanges at 208 K corresponding to i↔I, c or d↔C or D, d or c↔D or c, a↔b or B and/or A↔b or B, suggestive of interconversion of **2a** and **2b**. In principle, flexing of the diphosphine backbone, a 'waggling' of the CpW(CO)$_2$ group so as to place the Cp ligand over both WIr$_2$ faces remote from the diphosphine, or complete tripodal rotation will all interconvert **2a** and **2b**. However, the ^{31}P-NMR spectrum at 258 K, which reveals two distinct

P environments, is consistent with diphosphine backbone flexing being a very high energy process (coalescence of phosphorus resonances is not observed until > 300 K). Confirmatory evidence is provided by studies in the related tetrairidium system, which have shown that, for phosphines with variable oligomethylene backbone, flexing as proposed here does not become important until the backbone is lengthened to that of a butylene linkage [12]. We therefore reject diphosphine backbone flexing as the source of the low energy process. The presence of an h, H↔*e* crosspeak, indicating a **2a**, **2b**↔**2c** interconversion, is inconsistent with 'waggling' of the $CpW(CO)_2$ group at this temperature; although is possible that complete tripodal rotation (which involves placing the Cp ligand over the diphosphine-containing WIr_2 face) is slightly higher in energy than 'waggling' over the non-diphosphine-containing WIr_2 faces, no evidence for an energetic discrimination could be obtained with **2**. The EXSY data are thus consistent with tripodal rotation as the lowest energy process.

At 233 K a second process is observed, involving basal site exchange only (Fig. 5). The exchange e↔f↔c↔h↔d↔g↔e is consistent with the carbonyls exchanging via a concerted 'merry-go-round' process (n.b. the additional exchanges c or d↔d or c and f or g↔h suggest that the long mixing time used

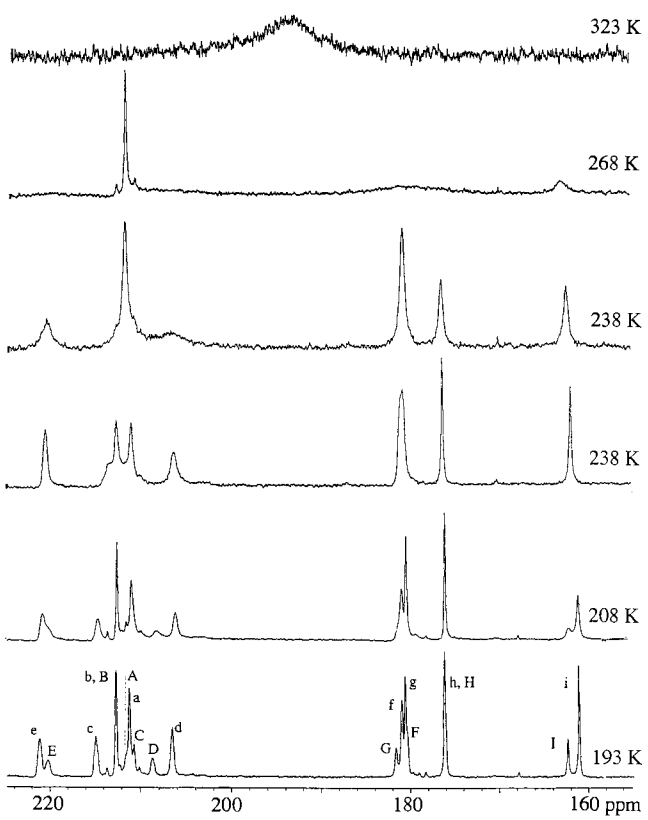

Fig. 2. Variable temperature ^{13}C-NMR spectroscopic study of [CpWIr_3(μ-dppe)(μ-$CO)_3(CO)_6$] (**2**).

for the experiment is such as to permit site exchange to succeeding sites).

A configuration of the related cluster [CpWIr_3(μ-dppm)(μ-$CO)_3(CO)_6$] (**3**) has also been structurally characterised; it is isostructural with **2b**, having a diaxially-ligated diphosphine and an apically-coordinated Cp ligand [3]. The ^{31}P-NMR spectrum of **3** at 298 K shows a broad singlet, which decoalesces upon cooling (Fig. 6). The spectrum at 181 K contains three signals, consistent with the presence of two isomers in the ratio 7:1. Similarly, the ^{13}C-NMR spectrum of **3** at 298 K is also very broad, but cooling to 181 K reveals resonances consistent with the presence of two isomers (Fig. 7). As with **2**, the signals in the ^{31}P- and ^{13}C-NMR spectra were assigned using the relationship between chemical shift and ligand position. The relative intensities of the resonances are consistent with the major isomer possessing geometry **3a**, the Cp ligand being inclined over the WIr_2 faces away from the diphosphine, and the minor isomer having geometry **3b**, with the Cp ligand inclined over the WIr_2 face including the diphosphine ligand (Fig. 8). At 181 K, resonances for the more abundant isomer **3a** are observed at 218.2 (e), 215.5 (a or b), 212.3 (c), 208.2 (b or a), 206.7 (d), 182.2 (f and g), 176.1 (h) and 164.1 (i) ppm, with relative intensities 1:1:1:1:1:2:1:1. Signals at 215.5 and 208.2 ppm show the expected satellite coupling to tungsten, and are therefore assigned to a and b. Carbonyl e, at 218.2 ppm, is assigned by analogy with the comparable carbonyl in **3b**. Resonances at 212.3 and 206.7 ppm are assigned to c and d, and labelled arbitrarily (as above). Assignments of f, g, h and i follow from our earlier discussion. Resonances for the least abundant isomer **3b** are observed at 228.4 (C), 210.2 (A and A′), 202.1 (B and B′), 180.4 (D and D′), 179.9 (E) and 170.6 (F) ppm, with relative intensities 1:2:2:2:1:1; the signals corresponding to A, A′ and B, B′ were assigned by comparison of their linewidths to previously assigned isomers above (resonances of bridging carbonyls are significantly broader than those of terminal carbonyls), and all other assignments follow logically from our earlier discussion. The assignment of the most downfield resonance as corresponding to C is straightforward (from its relative intensity); it confirms the assignment of the analogous carbonyl in the other isomers above. The assignment of isomers **3a** and **3b** is thus consistent with that of isomers **2a**–**c**. Significantly, the dppm ligand in **3** can only be configured symmetrically across the Ir–Ir bond, resulting in inequivalent P atoms in isomer **3a** and equivalent P atoms in **3b**. An EXSY spectrum at 183 K (Fig. 9) reveals the exchange pathway e↔f↔c↔h↔d↔g↔e in **3a**, and the analogous exchange (though less well resolved due to the decreased concentration) in **3b**, consistent with a merry-go-round of the six basal CO's. The exchanges a↔b and c↔d, and the lack of **3a**↔**3b** cross-peaks, are consistent with

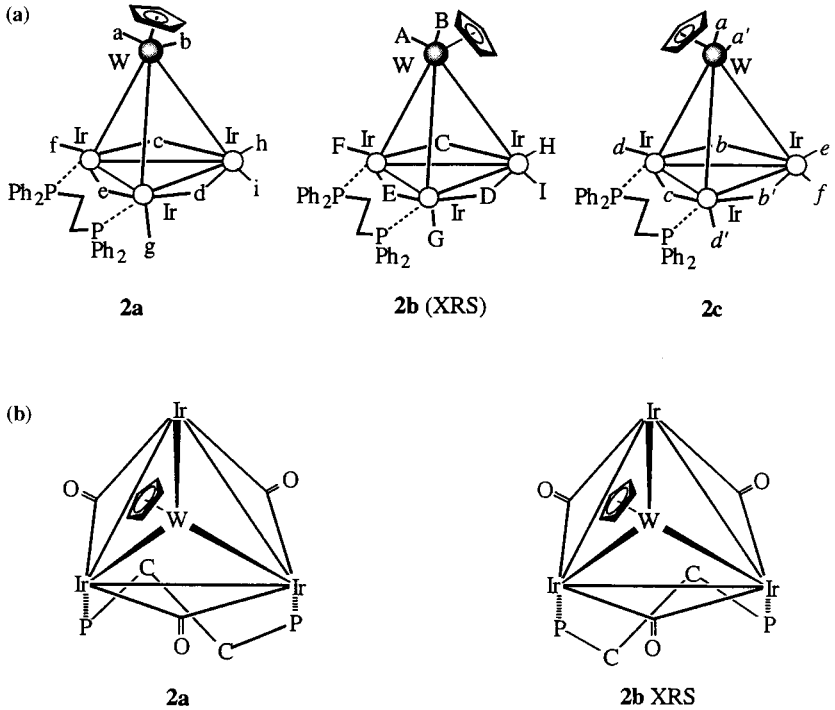

Fig. 3. Possible configurations for $[CpWIr_3(\mu\text{-dppe})(\mu\text{-}CO)_3(CO)_6]$ (**2**).

'waggling' of the $CpW(CO)_2$ group so as to place the Cp ligand over both WIr_2 faces remote from the diphosphine, but inconsistent with the onset of full tripodal rotation. Raising the temperature to 193 K results in the onset of full tripodal rotation, rendering isomers **3a** and **3b** equivalent (Fig. 10).

In our earlier reports of ligand substitution at tetrahedral tungsten–iridium and molybdenum–iridium clusters [1,3,4,8,9], we compared reactivity and product distribution to that observed in the parent tetrairidium system. The present results permit an assessment of the impact of apical metal replacement upon ligand fluxionality in tetrahedral clusters, by comparing data from the present work with that reported from fluxionality studies of disubstituted tetrairidium complexes with one edge-bridging bidentate ligand [13]. Studies of $[Ir_4(\mu\text{-L})(\mu\text{-}CO)_3(CO)_7]$ [L = dppm, dppp, dpam; dppp ≡ bis(diphenylphosphino)propane, dpam ≡ bis (diphenylarsino)methane] reveal fluxionality consistent with the lowest energy process being the merry-go-round of the six CO's about the basal plane perpendicular to the diaxially-coordinated ligands (Fig. 11, process 1). Upon raising the temperature, tripodal rotation at the non-phosphorus-ligated iridium in the basal plane of the bridge-opened intermediate occurs (process 2). Tripodal rotation at the apical iridium is the highest energy process observed (process 3). All site exchange processes are faster in the dppm-ligated cluster than in the dppp-containing cluster, rationalised by a greater relief of ring strain in proceeding to the unbridged intermediate (the Ir_4 core is smaller with an all-terminal ligand geometry than with an edge-bridged structure).

In the present work, a qualitative comparison of **2** and **3** reveals that signal broadening in the ^{13}C spectra occurs at a lower temperature in the dppm-containing cluster **3** than in its dppe-containing analogue **2**, consistent with results in the tetrairidium system. However, the lack of h↔i crosspeaks in the ^{13}C-EXSY spectra of **2** and **3** suggests that exchange pathway 2 in the tetrairidium system is not followed with these mixed-metal clusters (in the temperature range investigated); unlike the Ir_4 examples, it must be much higher in energy than process 3, a direct consequence of (conceptual) apical replacement of $Ir(CO)_3$ by $CpW(CO)_2$. Exchange pathway 3 is a lower energy process than or comparable energy process to pathway 1 in the mixed-metal system, and can be resolved into two processes in the case of **3**, the easier of which involves a 'waggling' of the $CpW(CO)_2$ vertex, and the more difficult of which involves placing the Cp ligand over the diphosphine-ligated WIr_2 face to effect complete tripodal rotation; again, the contrasting behaviour to that observed in the homometallic system is a consequence of apical metal replacement.

2.2. Syntheses and characterisation of complexes **4–9**

The reactions of $[CpWIr_3(CO)_{11}]$ (**1**) with n equivalents of $PMePh_2$ or PMe_2Ph ($n = 1–3$) proceed in dichloromethane at room temperature (r.t.) to afford the clusters $[CpWIr_3(\mu\text{-}CO)_3(CO)_{8-n}(PMePh_2)_n]$ [$n = 1$

(**4**), 2 (**5**) or 3 (**6**)] or $[CpWIr_3(\mu\text{-}CO)_3(CO)_{8-n}(PMe_2Ph)_n]$ [$n = 1$ (**7**), 2 (**8**) or 3 (**9**)], respectively, as the major or sole reaction products in good to excellent yields (40–76%). The clusters **4**–**9** have been characterised by a combination of IR, ^{1}H-, ^{13}C- and ^{31}P-NMR spectroscopies, MS and satisfactory microanalyses. IR spectra suggest the presence of edge-bridging carbonyl ligands in all complexes (ν(CO) 1801–1891 cm^{-1}), which contrasts with the all-terminal geometry of the precursor **1**. In combination with the X-ray structural results detailed below, the number of bands in the terminal carbonyl ligand ν(CO) regions of the IR spectra of **4**–**8** is indicative of the presence of isomers. The ^{1}H-NMR spectra contain signals assigned to Cp, phenyl and methyl groups for **4**–**9** in the appropriate ratios. The mass spectra of complexes **4**–**9** contain molecular ions, and all spectra contain fragment ions corresponding to stepwise loss of carbonyls; isotope patterns are consistent with the presence of three iridium atoms and one tungsten atom.

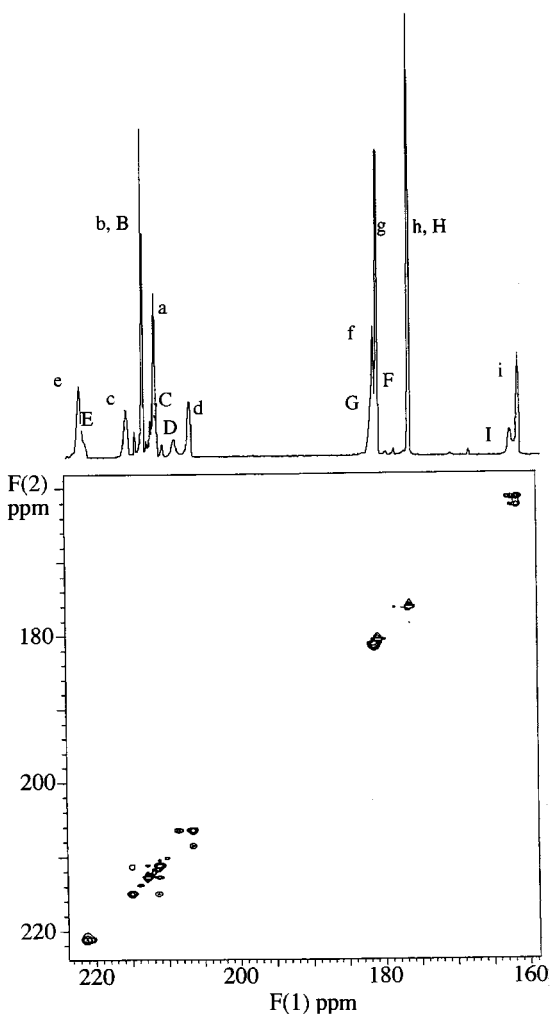

Fig. 4. ^{13}C-NMR EXSY spectrum of $[CpWIr_3(\mu\text{-dppe})(\mu\text{-}CO)_3(CO)_6]$ (**2**) at 208 K.

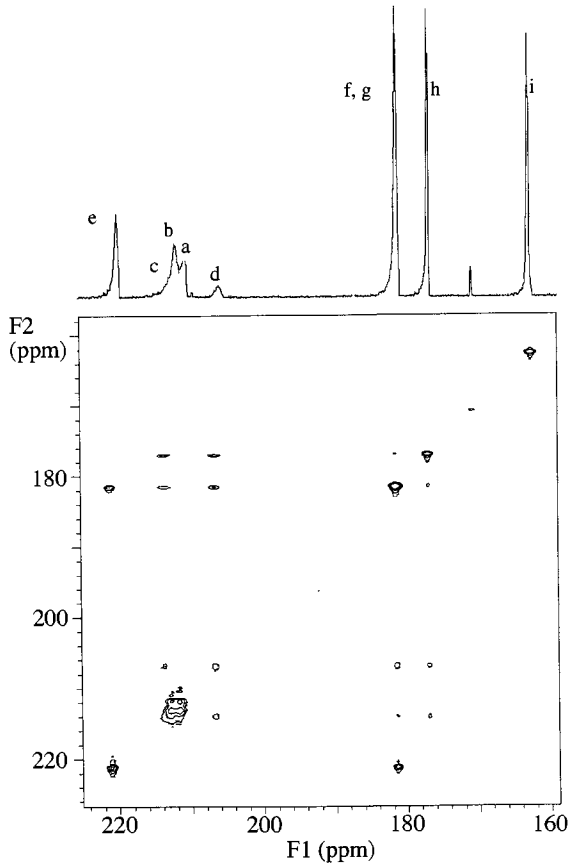

Fig. 5. ^{13}C-NMR EXSY spectrum of $[CpWIr_3(\mu\text{-dppe})(\mu\text{-}CO)_3(CO)_6]$ (**2**) at 233 K.

2.3. X-ray structural study of *7a*

The molecular structure of **7a** as determined by a single-crystal X-ray study is consistent with the formulation given above, defines the substitution sites of the phosphine, and aids interpretation of the ^{31}P-NMR spectra (see below). A summary of crystal and refinement data is found in Table 1, and selected bond distances and angles are listed in Table 2. An ORTEP plot showing the molecular geometry and atomic numbering scheme is shown in Fig. 12.

Complex **7a** has the WIr_3 pseudotetrahedral framework of the precursor cluster **1** and possesses an η^5-Cp group, three bridging carbonyls arranged about the triiridium plane, seven terminal carbonyl ligands, and an iridium-ligated dimethylphenylphosphine ligand. The WIr_3 core distances (W–Ir_{av} 2.85, Ir–Ir_{av} 2.75 Å) are slightly longer than those of **1** (W–Ir_{av} 2.82, Ir–Ir_{av} 2.70 Å); core distances of the mono(phosphine)-substituted complexes $[CpWIr_3(\mu\text{-}CO)_3(CO)_7(PPh_3)]$ and $[CpWIr_3(\mu\text{-}CO)_3(CO)_7(PMe_3)]$ [4] are also consistent with core expansion upon introduction of *p*-donor ligands. The longest W–Ir distance for **7a** is effectively *trans* to the Cp group. The Cp group is inclined towards a WIr_2 face; three W–C distances (average 2.29 Å) are shorter

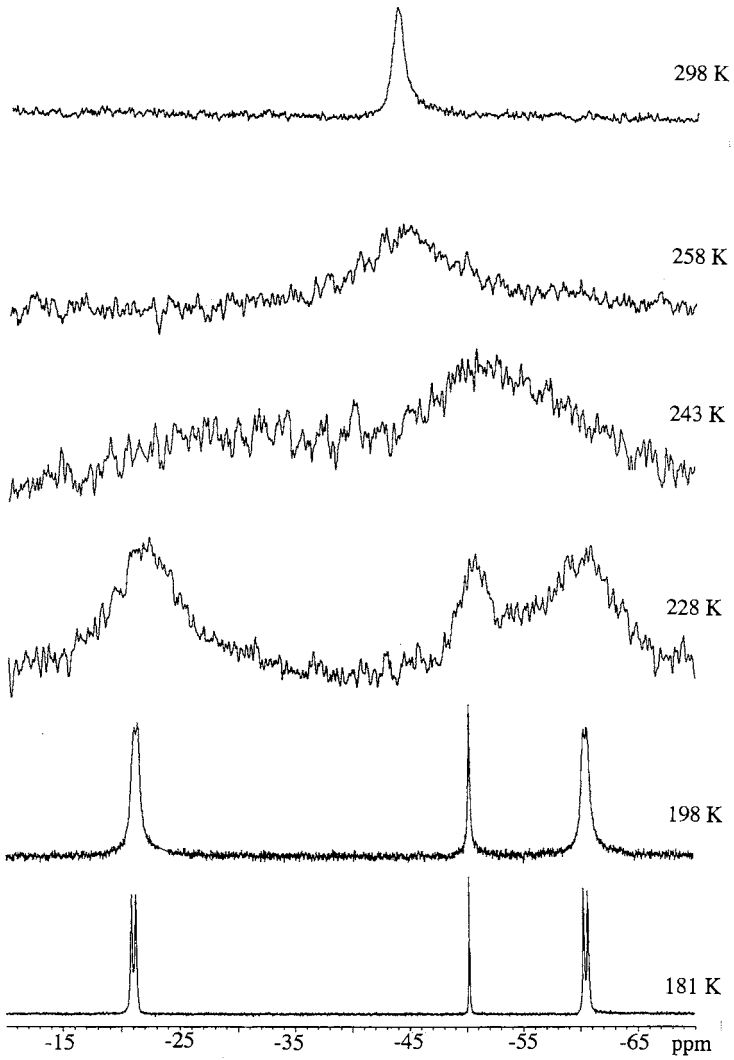

Fig. 6. Variable temperature ^{31}P-NMR spectroscopic study of [CpWIr$_3$(μ-dppm)(μ-CO)$_3$(CO)$_6$] (**3**).

than the two W–C distances (average 2.36 Å) involving the carbons closest to the Ir–Ir vector. Ir–CO(terminal) interactions [1.84(2)–1.91(2) Å] and W–CO interactions [1.96(2), 2.01(2) Å] for **7a** are unexceptional. The disposition of ligands in **7a** is similar to that found previously in [CpWIr$_3$(μ-CO)$_3$(CO)$_7$(PMe$_3$)] [4]. Formal electron counting reveals that **7a** has 60 e, electron precise for a tetrahedral cluster.

2.4. Discussion of isomers of **4**–**9**

The replacement of carbonyl by phosphine in the tungsten–triiridium system results in the carbonyl ligand geometry in the ground state shifting from all-terminal to one in which the three edges of one face of the tetrahedral core are spanned by bridging carbonyls, giving three different ligation sites with respect to this M$_3$(μ-CO)$_3$ plane, namely radial, axial and apical (Fig. 13). Although the least sterically hindered sites in tetrahedral clusters are the radial sites, most monosubstituted homometallic and heterometallic clusters have ligands in an axial site, presumably an electronic effect [14]. Homometallic cluster substitution then proceeds at a different basal metal to afford bis-substituted derivatives with radial, axial coordination for large ligands or diaxial coordination for small ligands. In contrast, the previously-reported clusters [CpWIr$_3$(μ-CO)$_3$(CO)$_7$(PPh$_3$)] and [CpWIr$_3$(μ-CO)$_3$(CO)$_7$(PMe$_3$)] exhibit radial, axial and/or axial, apical geometries [4]. The third incoming ligand in homometallic clusters occupies a basal coordination site to minimise steric effects, to give diradial, axial derivatives (most common) or radial, diaxial derivatives. In most cases the fourth ligand substitutes at the apical metal, forcing two ligands on the M$_{apical}$(M$_{basal}$)$_2$ face into axial sites and the remaining ligand into a radial site.

As mentioned above, the IR spectra of **4**–**8** are indicative of the presence of isomers. The ^{31}P-NMR spectra are also consistent with mixtures of isomers which interconvert on the NMR timescale. The r.t.

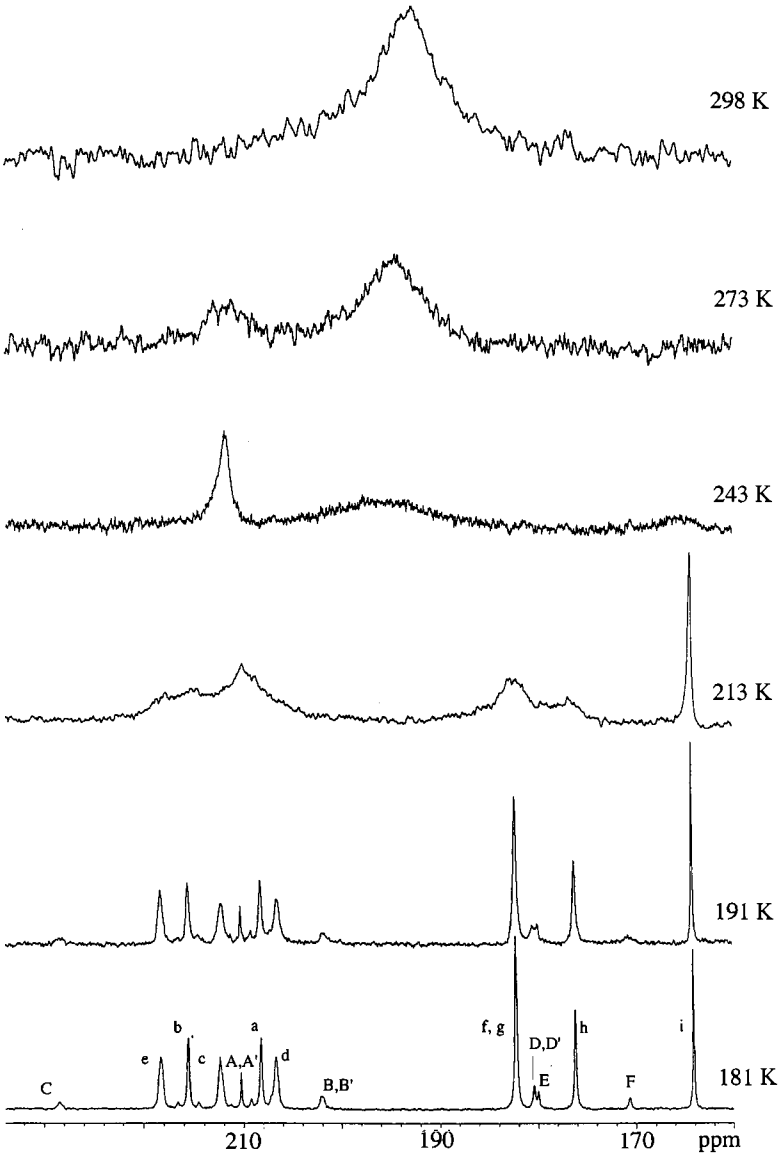

Fig. 7. Variable temperature ^{13}C-NMR spectroscopic study of [CpWIr$_3$(μ-dppm)(μ-CO)$_3$(CO)$_6$] (**3**).

^{31}P-NMR spectra of complexes contain either a broadened weighted average resonance, or no signal at all. In all cases, lowering the temperature sharpened the resonances, suggesting fluxionality in each derivative. The previously-reported triphenylphosphine- and trimethylphosphine-ligated tungsten–triiridium clusters exhibit different isomers [4]. To assess the importance of steric and electronic factors in governing isomer distribution, phosphines with cone angles and electronic parameters between the two outliers have now been investigated [electronic parameter ν (cm^{-1}): PPh_3 2068.9, $PMePh_2$ 2067.0, PMe_2Ph 2065.3, PMe_3 2064.1; cone angle θ (°): PPh_3 145, $PMePh_2$ 136, PMe_2Ph 122, PMe_3 118 [15]]. A summary of the resonances of all monodentate phosphine-substituted tungsten–iridium clusters is listed in Table 3, together with suggested coordination geometries (R, radial; Ax, axial; Ap, apical). The substitution sites of the new clusters [CpWIr$_3$(μ-CO)$_3$(CO)$_{8-n}$(L)$_n$] **4**–**9** have been assigned utilising information from (a) the crystallographically-

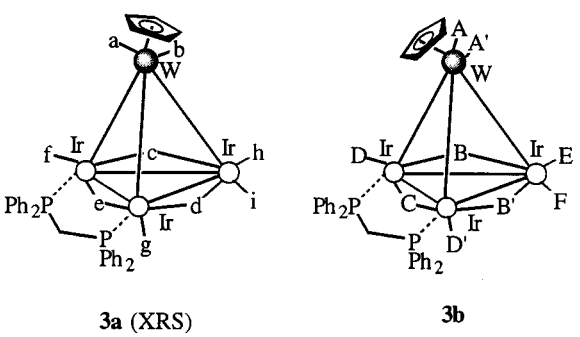

3a (XRS) **3b**

Fig. 8. Possible configurations for [CpWIr$_3$(μ-dppm)(μ-CO)$_3$(CO)$_6$] (**3**).

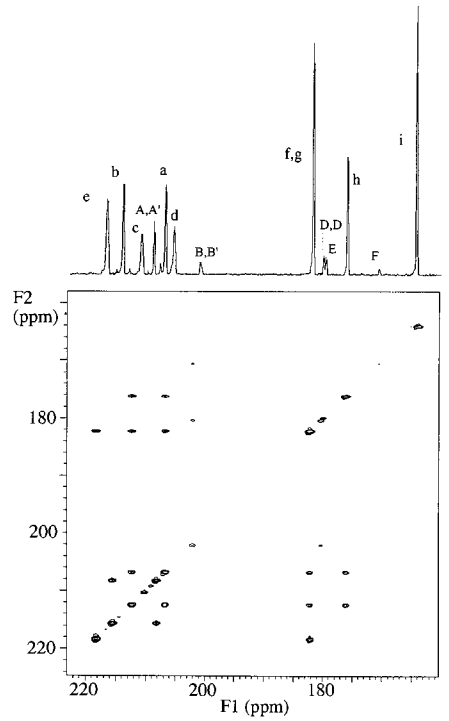

Fig. 9. ^{13}C-NMR EXSY spectrum of [$CpWIr_3(\mu$-dppm)(μ-$CO)_3(CO)_6$] (**3**) at 183 K.

verified isomer, (b) the substitution geometries found in the analogous triphenylphosphine- or trimethylphosphine-substituted tungsten–iridium clusters and (c) chemical shifts in the ^{31}P-NMR spectra.

Suggested geometries of all monodentate phosphine-substituted derivatives of [$CpWIr_3(CO)_{11}$] are given in Fig. 14. The crystallographically-observed **7a** has Cp occupying an apical site and PMe_2Ph occupying an axial site. This axial, apical geometry has previously been observed in an isomer of [$CpWIr_3(\mu$-$CO)_3(CO)_7(PMe_3)$]. The second isomer **7b**, with a radially coordinated phosphine, is consistent with the isomer adopting radial, axial geometry to minimise phosphine–Cp repulsion. This radial, axial isomer is found in both [$CpWIr_3(\mu$-$CO)_3(CO)_7(PPh_3)$] and [$CpWIr_3(\mu$-$CO)_3(CO)_7(PMe_3)$]. This assignment (and that for **4b**: see below) is the most tentative, though; low temperature spectra are somewhat broadened, and solid state ^{31}P-NMR spectra of [$CpMoIr_3$ (μ-$CO)_3(CO)_7(PPh_3)$] suggest that resonances assigned to radial, axial geometries may in fact be rapidly interconverting mixtures of isomers [8]. The shifts in the ^{31}P-NMR spectrum of **8** combined with the trisubstituted geometries characterised for [$CpWIr_3(\mu$-$CO)_3(CO)_6(PPh_3)_2$] and [$CpWIr_3(\mu$-$CO)_3(CO)_6(PMe_3)_2$] lead us to postulate isomer **8a** with radial, diaxial geometry and isomer **8b** with diradial, axial geometry. In contrast, clusters **2** and **3**, with insufficiently flexible diphosphine backbones, adopt diaxial, apical geometries (see above). The geometries adopted by the monodentate phosphine-containing clusters **8** and bidentate phosphine-containing clusters **2** and **3** are consistent with isomeric discrimination based on ligand size, as previously observed for homometallic clusters (see above); it should be noted, though, that the bidentate ligand-containing cluster geometries may be enforced by the ligand binding capabilities. NMR data for **9** shows the presence of one isomer, the shifts being consistent with a radial, diaxial, apical assignment, previously observed with [$CpWIr_3(\mu$-$CO)_3(CO)_5(PMe_3)_3$]. The suggested isomers for **4**–**6** follow analogously. Isomer **4a**, with an axially coordinated phosphine, is proposed to adopt an axial, apical geometry. Isomer **4b**, with a radially coordinated phosphine, presumably adopts the radial, axial geometry common to these systems (but see above). Chemical shifts in the ^{31}P-NMR spectrum of **5** again lead us to suggest the radial, diaxial geometry (**5a**) and the diradial, axial geometry (**5b**). The ^{31}P-NMR spectrum of **6**

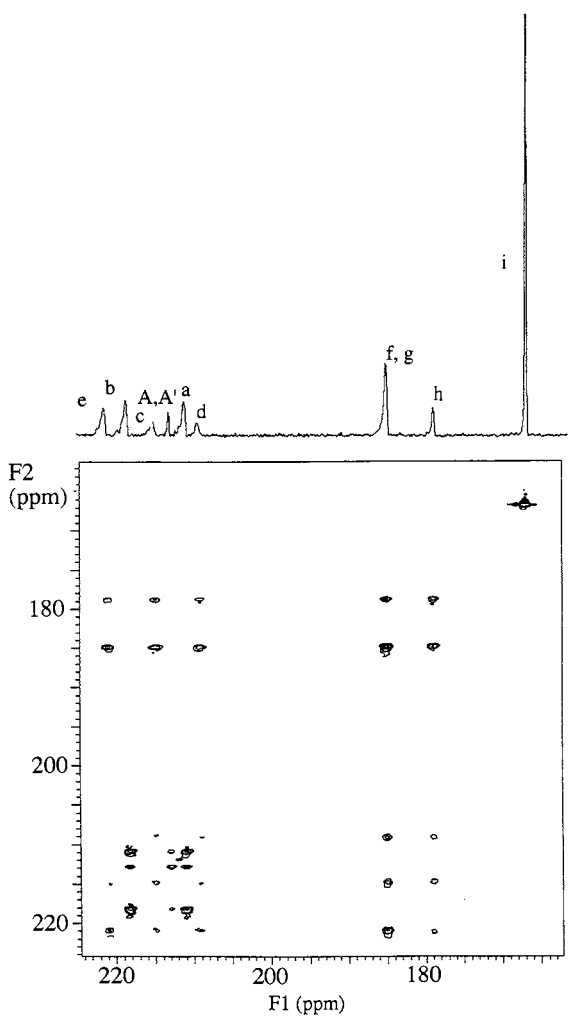

Fig. 10. ^{13}C-NMR EXSY spectrum of [$CpWIr_3(\mu$-dppm)(μ-$CO)_3(CO)_6$] (**3**) at 193 K.

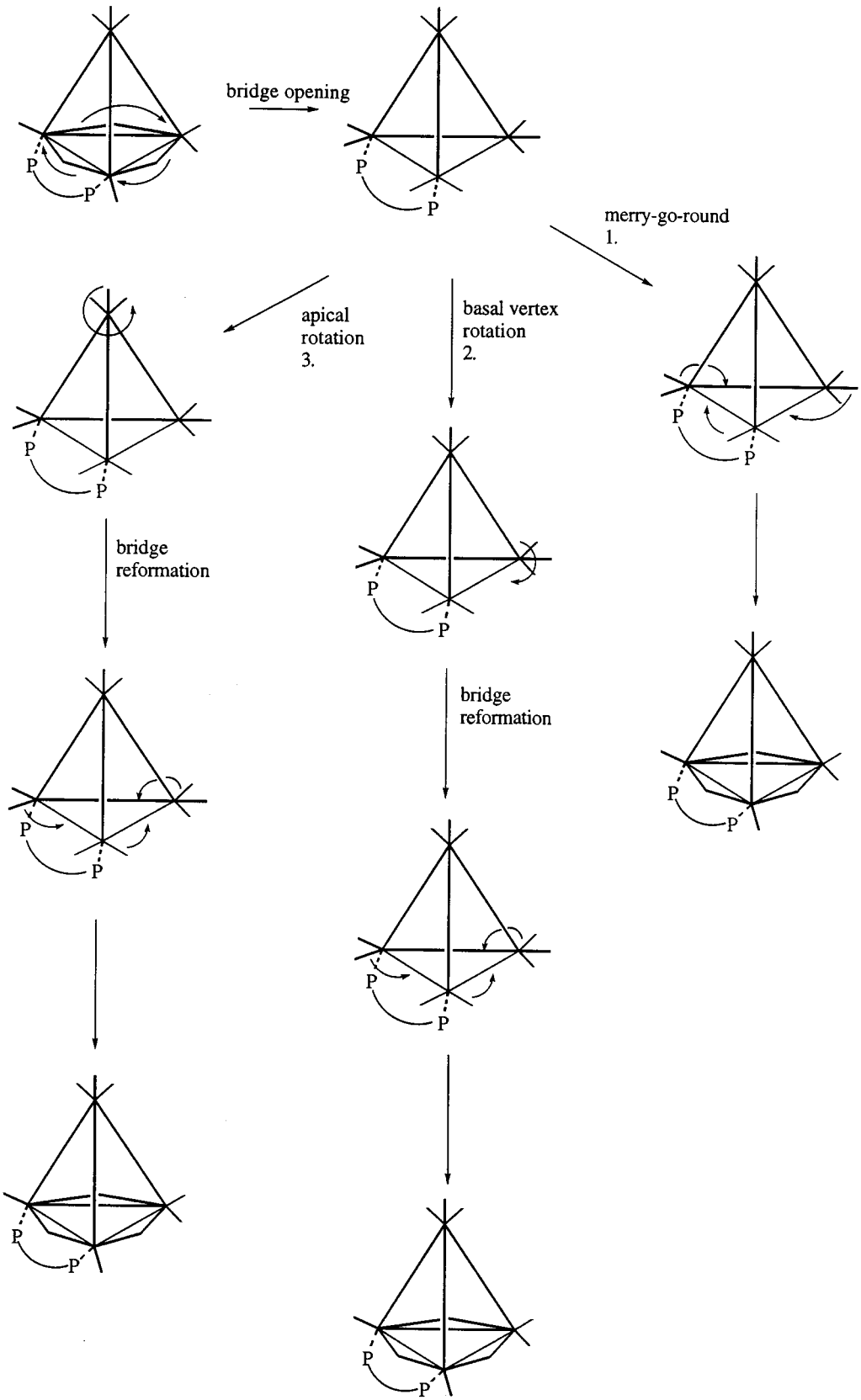

Fig. 11. CO exchange pathways in $[Ir_4(\mu\text{-L})(\mu\text{-CO})_3(CO)_7]$ (L = dppm, dppp, dpam).

Table 1
Crystallographic data for **7a**

Formula	$C_{23}H_{16}Ir_3O_{10}PW$
Formula weight	1243.86
Space group	$P2_1/n$ (no.14)
Crystal system	Monoclinic
a (Å)	9.602(1)
b (Å)	14.304(2)
c (Å)	20.114(2)
β (°)	97.864(9)
V (Å^3)	2736.5(6)
$D_{calc.}$ (g cm^{-3})	3.019
Z	4
μ (mm^{-1})	18.9
Specimen size (mm^3)	$0.20 \times 0.06 \times 0.04$
Abs. (min, max)	0.80, 1.00
$2\theta_{max}$ (°)	50.1
N	5065
N_o	2764
R	0.033
R_w	0.025

unusually suggests the presence of two isomers. The major isomer **6a**, with radial, axial and apical coordinated phosphines, is consistent with a radial, diaxial, apical assignment, seen previously with [$CpWIr_3(\mu$-$CO)_3(CO)_5(PMe_3)_3$]. The ^{31}P-NMR resonances for the minor isomer **6b** (two signals in the radial region of the spectrum in the ratio 2:1) can only be consistent with the isomer adopting triradial, apical geometry; the Cp adopts an apical position and is inclined over a WIr_2 face such that two of the phosphines are equivalent. This geometry was not observed with either [$CpWIr_3(\mu$-$CO)_3(CO)_8(PPh_3)_3$] or [$CpWIr_3(\mu$-$CO)_3(CO)_5(PMe_3)_3$], and is thus far unprecedented in structurally characterised tetrahedral clusters.

Table 2
Important bond lengths (Å) and angles (°) for complex **7a**

Bond lengths (Å)			
Ir(1)–Ir(2)	2.740(1)	Ir(1)–Ir(3)	2.752(1)
Ir(2)–Ir(3)	2.744(1)	Ir(1)–W(1)	2.823(1)
Ir(2)–W(1)	2.838(1)	Ir(3)–W(1)	2.9004(9)
Ir(3)–P(1)	2.327(4)	Ir(1)–C(1)	2.13(2)
Ir(1)–C(3)	2.02(2)	Ir(1)–C(21)	1.88(2)
Ir(1)–C(22)	1.91(2)	Ir(2)–C(1)	2.11(2)
Ir(2)–C(2)	2.13(2)	Ir(2)–C(11)	1.87(2)
Ir(2)–C(12)	1.87(2)	Ir(3)–C(2)	2.06(2)
Ir(3)–C(3)	2.06(2)	Ir(3)–C(31)	1.84(2)
W(1)–C(01)	2.27(2)	W(1)–C(02)	2.28(2)
W(1)–C(03)	2.33(2)	W(1)–C(04)	2.36(2)
W(1)–C(05)	2.36(2)	W(1)–C(41)	1.96(2)
W(1)–C(42)	2.01(2)		
Bond angles (°)			
Ir(2)–Ir(1)–Ir(3)	59.94(3)	Ir(2)–Ir(1)–W(1)	61.32(3)
Ir(3)–Ir(1)–W(1)	62.67(3)	Ir(1)–Ir(2)–Ir(3)	60.25(2)
Ir(1)–Ir(2)–W(1)	60.79(3)	Ir(3)–Ir(2)–W(1)	62.59(3)
Ir(1)–Ir(3)–Ir(2)	59.81(3)	Ir(1)–Ir(3)–W(1)	59.87(3)
Ir(2)–Ir(3)–W(1)	60.30(3)	Ir(1)–W(1)–Ir(2)	57.90(3)
Ir(1)–W(1)–Ir(3)	57.46(2)	Ir(2)–W(1)–Ir(3)	57.11(2)
Ir(1)–Ir(3)–P(1)	108.1(1)	Ir(2)–Ir(3)–P(1)	108.2(1)
W(1)–Ir(3)–P(1)	165.9(1)		

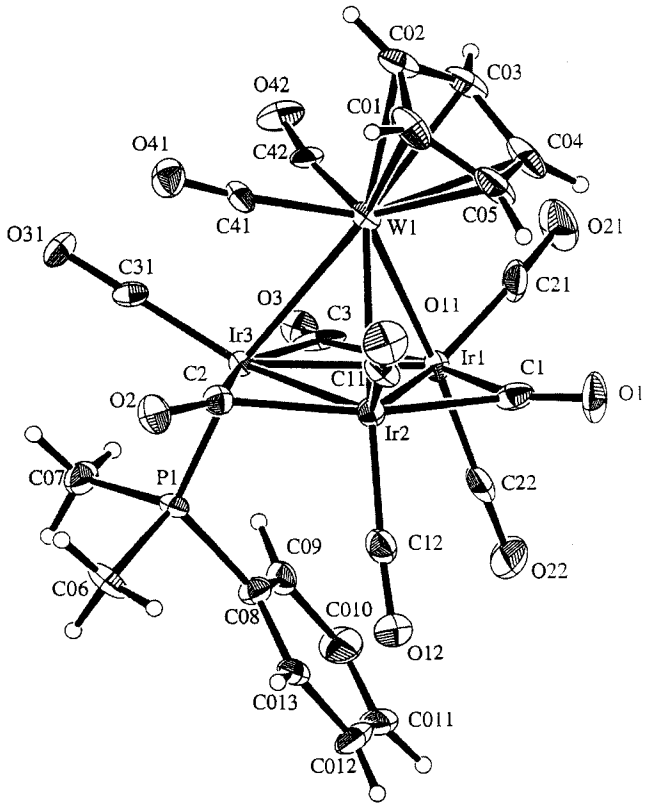

Fig. 12. Molecular structure and atomic labelling scheme for [Cp-$WIr_3(\mu$-$CO)_3(CO)_6(PMe_2Ph)$] (**7a**). Thermal envelopes (20%) are shown for the non-H atoms; H atoms have arbitrary radii of 0.1 Å.

3. Experimental details

All reactions were performed under an atmosphere of dry nitrogen (high purity grade, CIG), although no special precautions were taken to exclude air during work-up. The reaction solvent dichloromethane was dried over CaH_2; all other solvents were reagent grade,

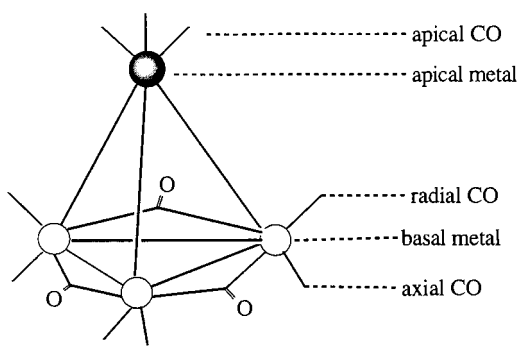

Fig. 13.

Table 3
^{31}P-NMR data for $[CpWIr_3(\mu\text{-}CO)_3(CO)_{8-n}(L)_n]$ ($L = PPh_3$, $PMePh_2$, PMe_2Ph, PMe_3; $n = 1–3$)

No. of ligands	Coordination site		^{31}P-NMR			
	P	Cp	PPh_3[a]	$PMePh_2$[b]	PMe_2Ph[b]	PMe_3[c]
2	R	Ax	4.7[d]	−18.2[e] (**4b**)	−25.8[f] (**7b**)	−26.1
	Ax	R	−5.1			
	Ax	Ap		−26.0[e] (**4a**)	−32.2[d,f] (**7a**)	−30.2[d]
3	R, Ax	Ax	25.2, −7.7[d]	−0.5, −22.9[e] (**5a**)	−18.9, −37.8[e] (**8a**)	−22.7, −38.7
	R, R	Ax	27.3	0.6[e] (**5b**)	−16.8[e] (**8b**)	−20.8
4	R, Ax, Ap	Ax		−3.6, −30.1, −55.3[e] (**6a**)	−21.2, −44.0, −72.8[e] (**9**)	−27.1, −45.2, −83.4
	R, R, Ap	Ax	31.8, −17.9 (2:1)			
	R, R, R	Ap		−8.9, −9.2 (2:1)[e] (**6b**)		

[a] R, radial; Ax, axial; Ap, apical. [b] This work. [c] See ref. [4]. [d] Crystallographically confirmed. [e] $CDCl_3$, 230 K. [f] d_6-Acetone, 213 K.

and used as received. Petroleum ether refers to a fraction of b.p. range 60–80°C. The products of thin-layer chromatography were separated on 20 × 20 cm glass plates coated with Merck GF_{254} silica gel (0.5 mm). $[CpWIr_3(CO)_{11}]$ [16], $[CpWIr_3(\mu\text{-dppe})(\mu\text{-}CO)_3(CO)_6]$ and $[CpWIr_3(\mu\text{-dppm})(\mu\text{-}CO)_3(CO)_6]$ [3] were prepared by the published procedures. Methyldiphenylphosphine, dimethylphenylphosphine, bis(diphenylphosphino)ethane and bis(diphenylphosphino)methane (Aldrich) were purchased commercially and used as received. The samples required for fluxionality studies were prepared from ^{13}CO-enriched (65%) $[CpWIr_3(CO)_{11}]$, the latter obtained by stirring a solution of the complex in CH_2Cl_2 under 1.2 atm ^{13}CO at 60°C for 48 h.

IR spectra were recorded on a Perkin-Elmer System 2000 Fourier transform spectrophotometer with CaF_2 optics. ^{1}H-NMR spectra were recorded on a Varian Gemini 300 spectrometer (300 MHz). The ^{13}C- and ^{31}P-NMR spectra were recorded on a Varian VXR300S spectrometer (^{13}C spectra at 75 MHz, ^{31}P spectra at 121 MHz) and are proton decoupled. Spectra were run in CD_2Cl_2, $CDCl_3$ or acetone-d_6 (Aldrich); chemical shifts in ppm are referenced to internal residual solvent for ^{1}H- and ^{13}C-NMR spectra and external 85% H_3PO_4 (0.0 ppm) for ^{31}P-NMR spectra. The $^{13}C\{^1H\}$-EXSY experiments were carried out using the standard NOESY pulse sequence with the mixing time set to 0.05 s. The ^{13}C-NMR spectra, when required for integration, were recorded with a recycle delay of 3–5 T_1. 2D-NMR spectra were recorded utilising a recycle delay of 1–3 T_1. T_1 measurements were performed using the inversion–recovery technique.

Mass spectra were obtained at the Australian National University on a VG ZAB 2SEQ instrument (30 kV Cs^+ ions, current 1 mA, accelerating potential 8 kV, matrix 3-nitrobenzyl alcohol). Peaks were recorded as m/z based on ^{183}W assignments and are reported in the form: m/z (assignment, relative intensity). Elemental microanalyses were performed by the Microanalysis Service Unit in the Research School of Chemistry, Australian National University.

3.1. Spectroscopic data for $[CpWIr_3(\mu\text{-dppe})(\mu\text{-}CO)_3CO)_6]$ (2)

^{13}C-NMR (CD_2Cl_2, 183 K): δ 227.9 (relative intensity 0.01, *c*), 221.5 (1, e), 220.5 (0.4, E), 215.0 (1, c), 212.4 (1.4, b and B), 211.2 (0.4, A), 211.0 (1, a), 210.7 (0.4, C), 210.1 (0.02, *a*, *a′*), 209.0 (0.4, D), 207.0 (1, d), 204.5 and 203.3 (0.02, *b* and *b′*), 181.8 (0.4, G), 181.0 (1, f), 180.5 (1, g), 180.2 (0.4, F), 179.5 and 178.9 (0.02, *d* and *d′*), 178.1 (0.01, *e*), 176.0 (1.4, h and H), 167.7 (0.01, *f*), 162.2 (0.4, I), 161.0 (1, i). ^{31}P-NMR (CD_2Cl_2, 183 K): δ 2.3 (s, 1P), −0.5 (s, 0.4P), −23.2 (s, 0.01P), −25.0 (s, 0.4P), −28.0 (s, 0.01P), −28.5 (s, 1P).

3.2. Spectroscopic data for $[CpWIr_3(\mu\text{-dppm})(\mu\text{-}CO)_3(CO)_6]$ (3)

^{13}C-NMR (CD_2Cl_2, 183 K): δ 228.4 (relative intensity 0.14, C), 218.2 (1, e), 215.5 (1, b), 212.3 (1, c), 210.2 (0.28, A and A′), 208.2 (1, a), 206.7 (1, d), 202.1 (0.28, B and B′), 182.2 (0.4, f and g), 180.4 (0.28, D and D′), 179.9 (0.14, E), 176.1 (1, h), 170.6 (0.14, F), 164.1 (1, i). ^{31}P-NMR (CD_2Cl_2, 183 K): δ −21.1 [d, $J(PP) = 44$ Hz, 1P], −50.2 (s, 0.28P), −60.5 [d, $J(PP) = 44$ Hz, 1P].

3.3. Reaction of $[CpWIr_3(CO)_{11}]$ with one equivalent of $PMePh_2$

An orange solution of $[CpWIr_3(CO)_{11}]$ (20.0 mg, 0.0176 mmol) and $PMePh_2$ (3.5 μl, 0.0175 mmol) in CH_2Cl_2 (20 ml) was stirred at r.t. for 24 h. The dark orange solution was then evaporated to dryness. The resultant orange residue was dissolved in CH_2Cl_2 (ca. 1 ml) and chromatographed (3 CH_2Cl_2:2 petroleum ether

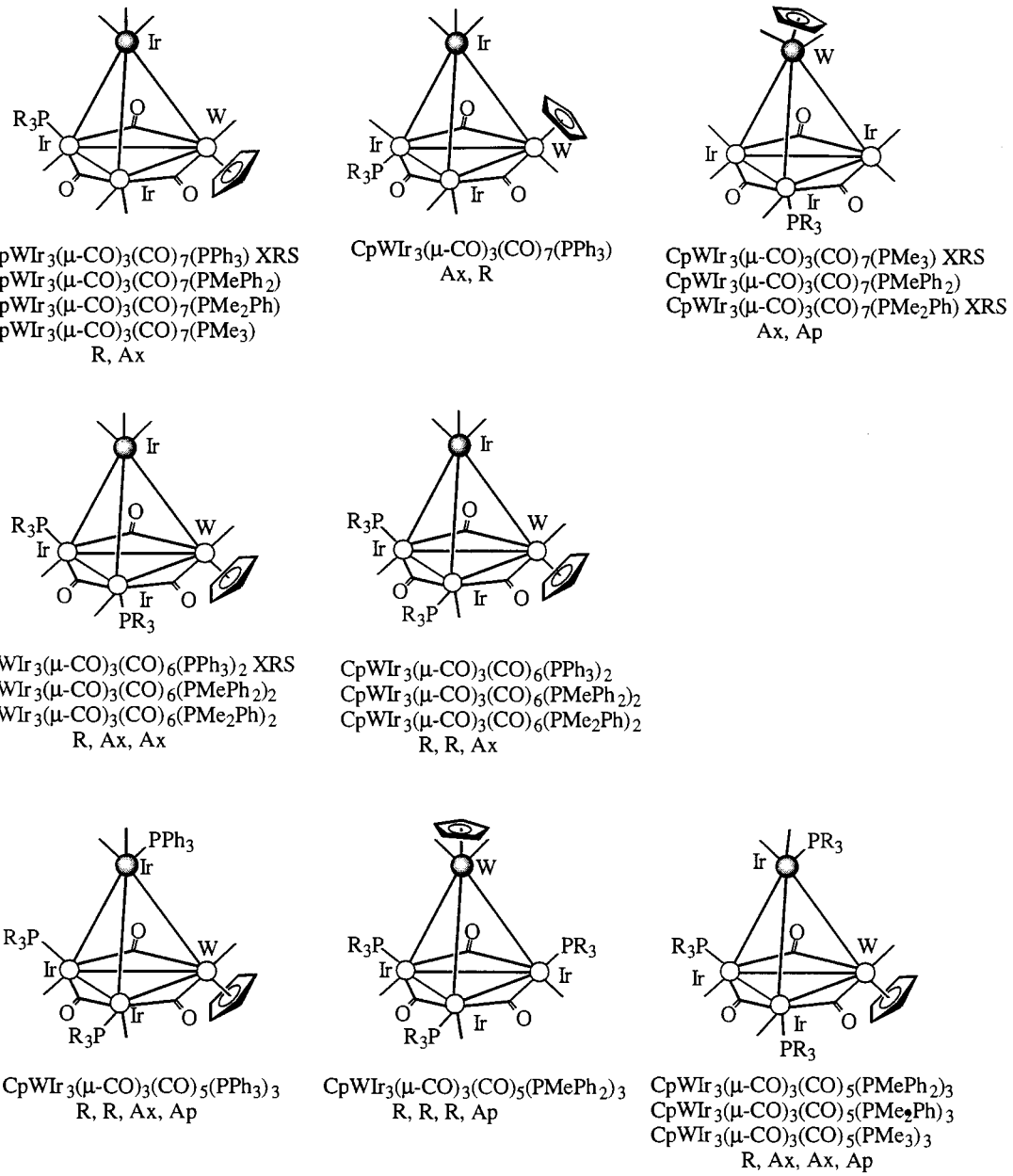

Fig. 14. Possible configurations for $[CpWIr_3(\mu\text{-}CO)_3(CO)_{8-n}(L)_n]$ ($L = PPh_3$, $PMePh_2$, PMe_2Ph, PMe_3; $n = 1–3$).

eluant), affording two bands. The contents of the first band were identified as **1** (1.3 mg, 6%) by solution IR spectroscopy. Crystallisation of the contents of the second band, R_f 0.55, from CH_2Cl_2/MeOH afforded orange crystals of $[CpWIr_3(\mu\text{-}CO)_3(CO)_7(PMePh_2)]$ (**4**) (12.4 mg, 54%).

Analytical data for **4**

IR (c-C_6H_{12}): 2074s, 2063m, 2042vs, 2031m, 2023vs, 2013vs, 2007vs, 1994vs, 1983m, 1970m, 1924m, 1878w, 1850w, 1825m, 1801m cm^{-1}. ^{1}H-NMR ($CDCl_3$): δ 7.56–7.42 (m, 10H, Ph), 4.90 [s (br), 5H, C_5H_5], 2.18 [d, J(HP) = 10 Hz, 3H, Me]. ^{13}C-NMR ($CDCl_3$): δ 134.2–128.7 (Ph), 85.8 (C_5H_5), 20.3 (Me). ^{31}P-NMR ($CDCl_3$, 230 K): δ −18.2 (s, 0.4P), −26.0 (s, 0.6P). FAB MS: 1306 ($[M]^+$, 10), 1278 ($[M-CO]^+$, 12), 1250 ($[M-2CO]^+$, 50), 1222 ($[M-3CO]^+$, 42), 1194 ($[M-4CO]^+$, 47), 1166 ($[M-5CO]^+$, 100), 1138 ($[M-6CO]^+$, 65), 1110 ($[M-7CO]^+$, 62), 1082 ($[M-8CO]^+$, 40). Anal. Calc.: C 25.75, H 1.39%. Found: C 25.48, H 1.63%.

3.4. Reaction of [CpWIr$_3$(CO)$_{11}$] with two equivalents of PMePh$_2$

Following the method of Section 3.1, $[CpWIr_3(CO)_{11}]$ (20.0 mg, 0.0176 mmol) and $PMePh_2$ (7.0 μl, 0.036 mmol) in CH_2Cl_2 (20 ml) afforded two bands after chromatography. The contents of the first band were

identified as **4** (3.3 mg, 12%) by solution IR spectroscopy. Crystallisation of the contents of the second band, R_f 0.40, from CH_2Cl_2/MeOH afforded orange crystals of $[CpWIr_3(\mu\text{-}CO)_3(CO)_6(PMePh_2)_2]$ (**5**) (11.2 mg, 43%).

Analytical data for **5**

IR (c-C_6H_{12}): 2059s, 2048m, 2036w, 2029m, 2001vs, 1992s, 1987vs, 1967m, 1901br m, 1869w, 1844w, 1810w cm^{-1}. ^{1}H-NMR ($CDCl_3$): δ 7.60–7.38 (m, 20H, Ph), 4.71 [s (br), 5H, C_5H_5], 2.06 [d, J(HP) = 10 Hz, 6H, Me]. ^{13}C-NMR ($CDCl_3$): δ 131.9–128.3 (Ph), 87.1 (C_5H_5), 20.2 (Me). ^{31}P-NMR ($CDCl_3$, 230 K): δ 0.6 (s, 0.8P), −0.5 (s, 0.6P), −22.9 (s, 0.6P). FAB MS: 1602 ($[M]^+$, 57), 1574 ($[M-CO]^+$, 54), 1546 ($[M-2CO]^+$, 69), 1518 ($[M-3CO]^+$, 100), 1490 ($[M-4CO]^+$, 42), 1462 ($[M-5CO]^+$, 100), 1434 ($[M-6CO]^+$, 64), 1406 ($[M-7CO]^+$, 58), 1378 ($[M-8CO]^+$, 40). Anal. Calc.: C 32.50, H 2.11%. Found: C 32.56, H 1.91%.

3.5. Reaction of $[CpWIr_3(CO)_{11}]$ with three equivalents of $PMePh_2$

Following the method of Section 3.1, $[CpWIr_3(CO)_{11}]$ (20.3 mg, 0.0178 mmol) and $PMePh_2$ (11 μl, 0.072 mmol) in CH_2Cl_2 (20 ml) afforded one band (R_f 0.51) after chromatography (2 CH_2Cl_2:1 petroleum ether eluant). Crystallisation from CH_2Cl_2/MeOH afforded orange crystals of $[CpWIr_3(\mu\text{-}CO)_3(CO)_5(PMePh_2)_3]$ (**6**) (20.0 mg, 76%).

Analytical data for **6**

IR (c-C_6H_{12}): 2012m, 1996s, 1992s, 1973vs, 1971vs, 1969sh, 1931br m, 1891m, 1869m cm^{-1}. ^{1}H-NMR ($CDCl_3$, 230 K): δ 7.66–7.14 (m, 36H, Ph), 5.28 (s, 1H, 0.5CH_2Cl_2), 4.37 (s, 5H, C_5H_5), 2.65–1.65 (m, 9H, Me). ^{13}C-NMR ($CDCl_3$): δ 131.9–128.3 (Ph), 87.1 (C_5H_5), 53.4 (CH_2Cl_2), 20.7 (Me). ^{31}P-NMR ($CDCl_3$, 230 K): δ −3.6 (s, 0.86P), −30.1 (s, 0.86P), −55.3 (s, 0.86P); −8.9 (s, 0.14P), −9.2 (s, 0.28P). FAB MS: 1602 ($[M]^+$, 57), 1574 ($[M-CO]^+$, 54), 1546 ($[M-2CO]^+$, 69), 1518 ($[M-3CO]^+$, 100), 1490 ($[M-4CO]^+$, 42), 1462 ($[M-5CO]^+$, 100), 1434 ($[M-6CO]^+$, 64), 1406 ($[M-7CO]^+$, 58), 1378 ($[M-8CO]^+$, 40). Anal. Calc.: C 32.50, H 2.11%. Found: C 32.56, H 1.91%.

3.6. Reaction of $[CpWIr_3(CO)_{11}]$ with one equivalent of PMe_2Ph

Following the method of Section 3.1, $[CpWIr_3(CO)_{11}]$ (20.0 mg, 0.0176 mmol) and PMe_2Ph (2.5 μl, 0.0175 mmol) in CH_2Cl_2 (20 ml) afforded two bands after chromatography. The contents of the first band were identified as **1** (1.9 mg, 9%) by solution IR spectroscopy. Crystallisation of the contents of the second band, R_f 0.61, from CH_2Cl_2/MeOH afforded orange crystals of $[CpWIr_3(\mu\text{-}CO)_3(CO)_7(PMe_2Ph)]$ (**7**) (14.8 mg, 64%).

Analytical data for **7**

IR (c-C_6H_{12}): 2071s, 2064w, 2042vs, 2032m, 2022vs, 2007vs, 1998m, 1993vs, 1960m, 1922m, 1824br m, 1801m cm^{-1}. ^{1}H-NMR ($CDCl_3$): δ 7.55–7.39 (m, 5H, Ph), 4.96 [s (br), 5H, C_5H_5], 2.18 [d, J(HP) = 10 Hz, 6H, Me]. ^{13}C-NMR ($CDCl_3$): δ 130.5–128.6 (Ph), 86.3 (C_5H_5), 20.0 (Me). ^{31}P-NMR ($CDCl_3$, 213 K): δ −25.8 (s, 0.67P), −32.2 (s, 0.33P). FAB MS: 1244 ($[M]^+$, 43), 1216 ($[M-CO]^+$, 74), 1188 ($[M-2CO]^+$, 45), 1160 ($[M-3CO]^+$, 51), 1132 ($[M-4CO]^+$, 37), 1104 ($[M-5CO]^+$, 100), 1076 ($[M-6CO]^+$, 73), 1048 ($[M-7CO]^+$, 80), 1020 ($[M-8CO]^+$, 51). Anal. Calc.: C 22.21, H 1.30%. Found: C 22.35, H 1.14%.

3.7. Reaction of $[CpWIr_3(CO)_{11}]$ with two equivalents of PMe_2Ph

Following the method of Section 3.1, $[CpWIr_3(CO)_{11}]$ (20.0 mg, 0.0176 mmol) and PMe_2Ph (4.8 μl, 0.0355 mmol) in CH_2Cl_2 (20 ml) afforded two bands after chromatography. The contents of the first band were identified as **7** (2.8 mg, 12%) by solution IR spectroscopy. Crystallisation of the contents of the second band, R_f 0.47, from CH_2Cl_2/MeOH afforded orange crystals of $[CpWIr_3(\mu\text{-}CO)_3(CO)_6(PMePh_2)_2]$ (**8**) (10.5 mg, 40%).

Analytical data for **8**

IR (c-C_6H_{12}): 2047m, 2043s, 2029w, 2010s, 1994vs, 1990m, 1977m, 1970m, 1956m, 1973w, 1899m, 1803w cm^{-1}. ^{1}H-NMR ($CDCl_3$): δ 7.66–7.35 (m, 10H, Ph), 4.89 [s (br), 5H, Cp], 2.23 [d, J(HP) = 10 Hz, 12H, Me]. ^{13}C-NMR ($CDCl_3$): δ 132.2–123.4 (Ph), 86.3 (C_5H_5), 20.4 (Me). ^{31}P-NMR ($CDCl_3$, 230 K): δ −16.8 (s, 1.72P), −18.9 (s, 0.14P), −37.8 (s, 0.14P). FAB MS: 1354 ($[M]^+$, 3), 1326 ($[M-CO]^+$, 10), 1298 ($[M-2CO]^+$, 25), 1270 ($[M-3CO]^+$, 100), 1242 ($[M-4CO]^+$, 12), 1214 ($[M-5CO]^+$, 60), 1186 ($[M-6CO]^+$, 79), 1158 ($[M-7CO]^+$, 50), 1130 ($[M-8CO]^+$, 20). Anal. Calc.: C 26.61, H 1.67%. Found: C 26.82, H 1.67%.

3.8. Reaction of $[CpWIr_3(CO)_{11}]$ with three equivalents of PMe_2Ph

Following the method of Section 3.1, $[CpWIr_3(CO)_{11}]$ (20.3 mg, 0.0178 mmol) and PMe_2Ph (7.0 μl, 0.071 mmol) in CH_2Cl_2 (20 ml) afforded one band (R_f 0.43) after chromatography (2 CH_2Cl_2:1 petroleum ether eluant). Crystallisation from CH_2Cl_2/MeOH afforded orange crystals of $[CpWIr_3(\mu\text{-}CO)_3(CO)_5(PMe_2Ph)_3]$ (**9**) (13.5 mg, 52%).

Analytical data for **9**

IR (c-C_6H_{12}): 2006s, 1992w, 1968sh, 1967vs, 1952s, 1915w, 1861w, 1825w cm^{-1}. ^{1}H-NMR ($CDCl_3$, 230K): δ 7.72–7.20 (m, 15H, Ph), 5.28 (s, 1H, 0.5CH_2Cl_2), 4.38 (s, 5H, C_5H_5), 2.26–1.17 (m, 18H, Me). ^{13}C-NMR

($CDCl_3$): δ 129.5–127.8 (Ph), 87.1 (C_5H_5), 53.4 (CH_2Cl_2), 20.4 (Me). ^{31}P-NMR ($CDCl_3$, 230 K): δ −21.2 (s, 1P), −44.0 (s, 1P), −72.8 (s, 1P). FAB MS: 1464 ($[M]^+$, 10), 1408 ($[M-2CO]^+$, 29), 1380 ($[M-3CO]^+$, 100), 1353 ($[M-4CO]^+$, 17), 1324 ($[M-5CO]^+$, 53), 1296 ($[M-6CO]^+$, 61), 1268 ($[M-7CO]^+$, 10). Anal. Calc.: C 29.90, H 2.61%. Found: C 29.68, H 1.19%.

3.9. Structure determination

Crystals of compound **7** suitable for diffraction analysis were grown by slow diffusion of methanol into dichloromethane at −5°C. A unique diffractometer data set was measured at ca. 295 K within the specified $2\theta_{max}$ limit ($2\theta/\theta$ scan mode; monochromatic Mo–K_α radiation ($\lambda = 0.71073$ Å), yielding N independent reflections. N_o of these with $I > 3\sigma(I)$ were considered 'observed' and used in the full matrix/large block least squares refinements after analytical absorption correction. Anisotropic thermal parameters were refined for the non-H atoms; $(x, y, z, U_{iso})_H$ were included, constrained at estimated values. Conventional residuals R, R_w on $|F|$ at convergence are given. Neutral atom complex scattering factors were used, computation using teXsan [17]. Pertinent results are given in the figures and tables. Atomic coordinates, bond lengths and angles, and thermal parameters have been deposited at the Cambridge Structural Database.

Acknowledgements

We thank the Australian Research Council for support of this work and Johnson-Matthey Technology Centre for the generous loan of $IrCl_3$. M.G. Humphrey is an ARC Australian Research Fellow.

References

[1] S.M. Waterman, M.G. Humphrey, D.C.R. Hockless, J. Organomet. Chem. 555 (1998) 25.
[2] Comprehensive Organometallic Chemistry II, vol. 10, E.W. Abel, F.G.A. Stone, G. Wilkinson (Eds.), Pergamon, Oxford, UK, 1995.
[3] J. Lee, M.G. Humphrey, D.C.R. Hockless, B.W. Skelton, A.H. White, Organometalllics 12 (1993) 3468.
[4] S.M. Waterman, M.G. Humphrey, V.-A. Tolhurst, B.W. Skelton, A.H. White, Organometallics 15 (1995) 934.
[5] S.M. Waterman, M.G. Humphrey, V.-A. Tolhurst, B.W. Skelton, A.H. White, J. Organomet. Chem. 507 (1995) 163.
[6] S.M. Waterman, M.G. Humphrey, D.C.R. Hockless, Organometallics 15 (1995) 1745.
[7] N.T. Lucas, M.G. Humphrey, D.C.R. Hockless, J. Organomet. Chem. 535 (1997) 175.
[8] N.T. Lucas, I.R. Whittall, M.G. Humphrey, D.C.R. Hockless, M.P.S. Perera, M.L. Williams, J. Organomet Chem. 540 (1997) 147.
[9] N.T. Lucas, M.G. Humphrey, M.L Williams, P.C. Healy, J. Organomet. Chem. 519 (1997) 545.
[10] R. Ros, A. Scrivanti, V.G. Albano, D. Braga, J. Chem. Soc. Dalton Trans. (1986) 2411.
[11] A.E. Derome, Modern NMR Techniques for Chemistry Research, Pergamon, Oxford, 1987.
[12] A. Strawczynski, R. Ros, R. Roulet, D. Braga, C. Gradella, F. Grepioni, Inorg. Chim. Acta 170 (1990) 17.
[13] A. Strawczynski, G. Suardi, R. Ros, R. Roulet, Helv. Chim. Acta 76 (1993) 2210.
[14] M. Bojczuk, B.T. Heaton, S. Johnson, C.A. Ghilardi, A. Orlandini, J. Organomet. Chem. 341 (1988) 473.
[15] C.A. Tolman, Chem. Rev. 77 (1977) 313.
[16] J.R. Shapley, S.J. Hardwick, D.S. Foose, G.D. Stucky, J. Am. Chem. Soc. 103 (1981) 7383.
[17] teXsan: Single Crystal Structure Analysis Software, Version 1.7-3, Molecular Structure Corporation, The Woodlands, TX, USA, 1995.